Structural Basis for Thermal Stability of Human Low-Density Lipoprotein†

Shobini Jayaraman, Donald Gantz, and Olga Gursky*

Department of Physiology and Biophysics, W329, Boston University School of Medicine, 715 Albany Street, Boston, Massachusetts 02118

Received November 29, 2004; Revised Manuscript Received January 6, 2005

ABSTRACT: The stability of human low-density lipoprotein (LDL), the major cholesterol carrier in plasma, was analyzed by heating samples of different concentrations at a rate from 11 to 90 K/h. Correlation of the calorimetric, circular dichroism, fluorescence, turbidity, and electron microscopic data shows that thermal disruption of LDL involves irreversible changes in the particle morphology and protein conformation but no global protein unfolding. Heating to 85 °C induces LDL conversion into smaller and larger particles and apparent partial dissociation, but not unfolding, of its sole protein, apoB. Further heating leads to partial unfolding of the β-sheets in apoB and to fusion of the protein-depleted LDL into large aggregated lipid droplets, resulting in a previously unidentified high-temperature calorimetric peak. These lipid droplets resemble in size and morphology the extracellular lipid deposits formed in the arterial wall in early atherosclerosis. The strong concentration dependence of LDL fusion revealed by near-UV/visible CD, turbidity, and calorimetry indicates high reaction order, and the heating rate dependence suggests high activation energy that arises from transient disruption of lipid and/or protein packing interactions in the course of particle fusion and apparent apoB dissociation. Consequently, thermal stability of LDL is modulated by kinetic barriers. Similar barriers may confer structural integrity to LDL subclasses in vivo.

Low-density lipoproteins deliver cholesterol to peripheral tissues. LDL[1] are macromolecular complexes that contain an apolar core of cholesterol esters (CE) and triacylglycerides (TG) and an amphipathic surface that imparts the particle solubility and is comprised mainly of apolipoprotein B (apoB) in a cholesterol-containing phospholipid monolayer (*1*−*4*). Plasma levels of LDL correlate with the incidence of atherosclerosis, which is the leading cause of death in western society (reviewed in refs *5*−*7*). Different pathways of LDL production from very low density and intermediate density lipoproteins, along with enzymatic modifications (*8*−*10*), contribute to the formation of discrete LDL subclasses differing in size, density, lipid composition, apoB conformation, and metabolic properties (*11*, *12*). Small dense LDL form a particularly atherogenic subclass; this is due, in part, to the altered apoB conformation that makes small LDL particularly vulnerable to oxidation and increases their affinity for arterial proteoglycans (*8*, *9*, *11*, *13*). LDL retention by the proteoglycans in the arterial wall is the key initiating step in atherosclerosis (*14*). It generates a cascade of responses including proatherogenic LDL modifications such as oxidation, fusion, and formation of extracellular lipid droplets, leading to early atherosclerotic lesions and to an increased LDL uptake by macrophages (*2*, *10*, *15*, *16*). Our aim is to provide the energetic and structural basis for LDL stability and morphological transitions.

Earlier studies of LDL stability revealed an irreversible calorimetric transition near 80 °C accompanied by an increase in turbidity (*17*, *18*), which was attributed to apoB unfolding and particle disruption (*19*−*25*). This increased turbidity, which reflects morphological changes in LDL involving a release of CE lipid droplets, has limited the circular dichroism (CD) secondary structural analysis of LDL to 70 °C (*21*, *26*). However, infrared spectroscopy suggests that LDL heating to 85 °C does not increase the random coil content in apoB (*22*). Thus, the structural basis for the LDL transition near 80 °C is unclear.

The energetic basis for LDL stability is also unclear, since the irreversibility of the high-temperature calorimetric transition has precluded its thermodynamic analysis. Irreversible heat-induced transitions have also been observed in high-density plasma lipoproteins (HDL). The first of these transitions involves dissociation, but not unfolding, of the major HDL protein, apolipoprotein A-1 (apoA-1), and consequent fusion of the protein-depleted HDL that compensates for the reduced polar surface; the second transition involves dissociation of a highly hydrophobic apolipoprotein A-2 (apoA-2), HDL rupture, and release of the apolar core lipids (*27*−*29*). These morphological transitions are associated with high kinetic barriers that confer HDL stability and may modulate HDL metabolism (*29*−*31*). We hypothesize that thermal disruption of LDL may also be a kinetically controlled reaction that involves protein dissociation and changes in the particle morphology. However, the structural bases for the stability of HDL and LDL are expected to differ, since one HDL particle contains 200−400 lipid molecules

† This work was supported by NIH Grant GM67260 to O.G. The CD spectroscopy, calorimetry, electron microscopy, and protein biochemistry core facilities are supported by NIH Program Project Grant HL26355 (D. Atkinson, Program Director).

* Corresponding author. Phone: (617) 638-7894. Fax: (617) 638-4207. E-mail: gursky@bu.edu.

[1] Abbreviations: LDL, low-density lipoprotein; HDL, high-density lipoprotein; apoB, apolipoprotein B; apoA-1, apolipoprotein A-1; apoA-2, apolipoprotein A-2; CE, cholesterol ester; TG, triglyceride; DSC, differential scanning calorimetry; CD, circular dichroism; EM, electron microscopy; TLC, thin-layer chromatography.

10.1021/bi047493v CCC: $30.25
Published on Web 02/17/2005

and two to four copies of water-soluble apoA-1 (243 amino acids) and other exchangeable apolipoproteins, while the LDL particle contains about 3000 lipid molecules and a single copy of water-insoluble apoB (4536 amino acids). To test this hypothesis, we analyze the heat-induced structural changes in LDL by using differential scanning calorimetry (DSC), CD and fluorescence spectroscopy, turbidity measurements, and electron microscopy (EM).

MATERIALS AND METHODS

Lipoprotein Preparation and Characterization. LDL from four healthy volunteer donors were used in this study. Single-donor LDL were isolated from EDTA-treated plasma by density-gradient ultracentrifugation at a density range of 1.019−1.063 g/mL (*32*). LDL purity determined by agarose gel electrophoresis was 95%. An LDL solution of 4−5 mg/mL protein concentration was dialyzed against standard buffer (10 mM sodium phosphate, 0.25 mM NaEDTA, 0.02% NaN_3, pH 7.7), degassed, and stored in the dark at 4 °C. The stock solution was used in 1−2 weeks during which no protein degradation (assessed by SDS gel electrophoresis) or LDL oxidation [assessed by UV absorption at 234 nm, thin-layer chromatography (TLC), agarose gel electrophoresis, and ^{31}P NMR (*33*, *34*)] was detected. Briefly, ^{1}H-decoupled ^{31}P NMR spectra of LDL in 5 mM Tris buffer were obtained in 10 mm tubes with a Bruker AMX-300 spectrometer at 25 °C, and the chemical shifts were determined relative to the resonance position of 85% H_3PO_4 as an external standard.

Differential Scanning Calorimetry. An upgraded MC2 microcalorimeter (MicroCal, Amherst, MA) was used to record the heat capacity $C_p(T)$ as described (*29*). The data were recorded from degassed LDL solutions of 3.3−3.7 mg/mL protein concentration during heating at a rate of 90 K/h under N_2 pressure of 20 psi. Buffer baselines were subtracted. ORIGIN software was used for the data collection and analysis.

CD Spectroscopy and Light Scattering. AVIV 215 and 62DS spectrometers were used to record far-UV (185−250 nm) and near-UV/visible (250−520 nm) CD data. Heat-induced turbidity changes were monitored by dynode voltage as described (*29*, *31*). The CD spectra were recorded from degassed LDL solutions (20−40 μg/mL protein concentrations for far-UV and 1.5−4.0 mg/mL for near-UV) using 30−60 s/nm accumulation time. The CD and turbidity melting curves were recorded at 220 and 280 nm during sample heating and cooling with 1 °C increment at a rate from 80 to 10 K/h. The CD data are expressed as molar residue ellipticity, [Θ].

Electron Microscopy. LDL subjected to various thermal treatments were visualized at 22 °C by negative staining electron microscopy as described (*30*, *31*) using a CM12 transmission electron microscope (Philips Electron Optics). Particle size analysis was carried out in PHOTOSHOP computer graphics using 200−400 particles.

Fluorescence Spectroscopy. Trp emission spectra of LDL (10−20 μg/mL protein concentration) subjected to various thermal treatments were recorded using a FluoroMax-2 spectrofluorometer as described (*29*). Spectra were recorded from 315 to 540 nm using 5 nm excitation and emission slit widths and 296 nm excitation wavelength. The wavelength of the emission maximum was determined with 2 nm accuracy. All experiments in this study were repeated four to eight times.

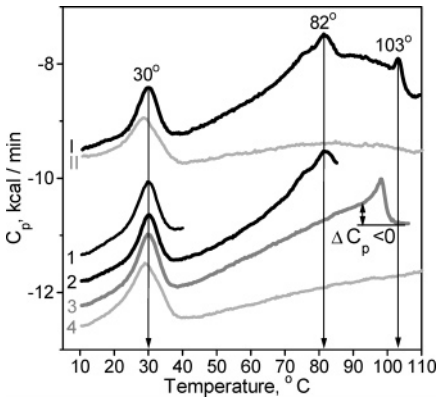

FIGURE 1: Excess heat capacity $C_p(T)$ of LDL recorded by DSC. The protein concentration is 3.7 mg/mL, and the heating rate is 90 K/h. The data are shifted along the *Y*-axis to avoid overlap. Curves I and II are the first and second scans recorded upon sample heating from 5 to 115 °C. Arrows indicate peak temperatures in curve I. Curves 1−4 were recorded from an identical LDL sample upon heating from 5 °C to incrementally increasing temperatures, followed by 1 h incubation at 5 °C: 1, 40 °C; 2, 85 °C; 3, 106 °C; 4, 115 °C.

RESULTS

Figure 1 shows the heat capacity of LDL recorded in sequential scans during heating from 5 to 115 °C at 90 K/h. The first scan (curve I) shows a peak at 30 °C corresponding to smectic-to-disorder transition in CE/TG (*17*−*19*, *23*) and two high-temperature peaks. The first peak, which is centered at 82 °C with a shoulder near 75 °C, has been attributed to apoB denaturation (*19*−*25*). The second previously unidentified peak is invariant for LDL samples of similar concentration from the same plasma pool but shows variable amplitudes and peak temperatures for LDL from different pools (92−105 °C), suggesting the effects of the diet-dependent lipid composition. The absence of the high-temperature transitions from the next scan (curve II) indicates their irreversibility, and the −1.5 °C shift and broadening of the CE/TG peak in curve II, which was observed before (*17*, *18*, *21*), indicate altered packing of apolar lipids after LDL heating to 115 °C.

To probe the physical origin and the reversibility of the individual DSC transitions, the Cp(T) data were recorded from another LDL sample under otherwise identical conditions during heating from 5 °C to incrementally increasing temperatures, followed by cooling and incubation at 5 °C (Figure 1, curves 1−4). Heating to 40 °C (completion of the CE/TG peak) is reversible (*17*, *18*, *21*), as evident from full superimposition of the CE/TG peaks in curves 1 and 2. Also, heating and cooling from 5 to 40 °C cause no changes in the peak at 82 °C (curves 2 and I compared). In contrast, heating to 85 °C (completion of the first high-temperature peak) eliminates this peak from the next scan and shifts the temperature of the second high-temperature peak by −5 °C (curve 3). Thus, the first high-temperature transition is irreversible, and the second transition is affected by the thermal history of the sample, indicating complex kinetics of the underlying structural changes. The negative apparent heat capacity increment in the second transition (Figure 1,

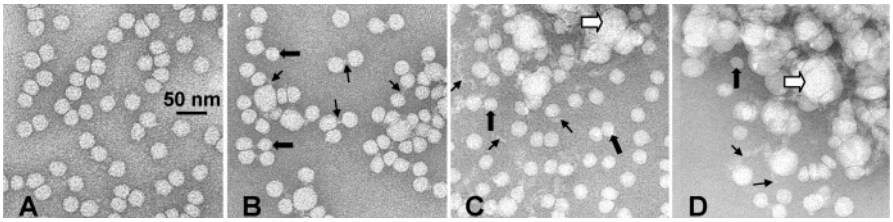

FIGURE 2: Electron micrographs of negatively stained LDL at various stages of thermal disruption. LDL solutions (3.7 mg/mL protein concentration) were heated at 90 K/h to 75−115 °C. The micrographs were recorded at 22 °C after heating to (A) 75 °C (the particles appear identical to intact LDL), (B) 85 °C, (C) 100 °C, and (D) 115 °C. Small LDL-like particles (thick arrows), lipid droplets (open arrows), and dissociated apoB (thin arrows) are indicated.

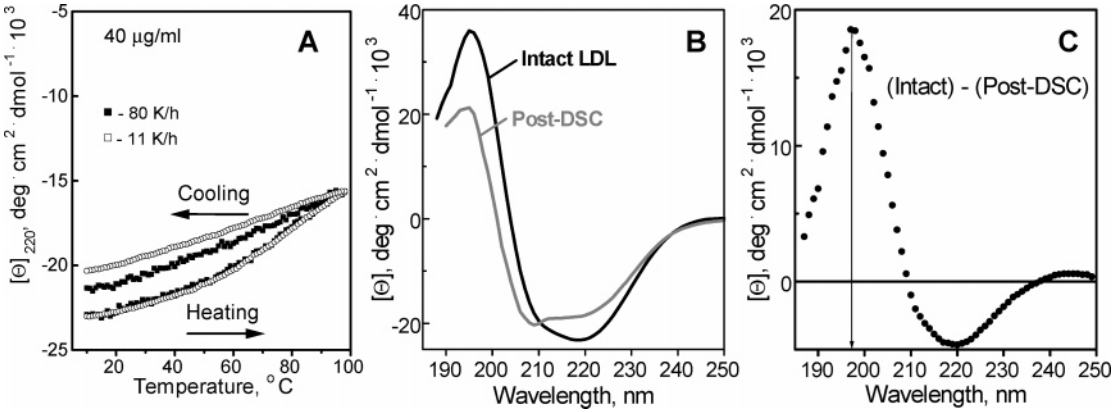

FIGURE 3: Heat effects on the protein secondary structure in LDL. The protein concentration is 40 μg/mL. (A) CD melting curves recorded at 220 nm of intact LDL upon heating and cooling at a rate 11 K/h (□) and 80 K/h (■). (B) Far-UV CD spectra of LDL recorded at 25 °C before (black line) and after (gray line) heating to 115 °C; an LDL sample (3.7 mg/mL protein concentration) was heated from 5 to 115 °C at 90 K/h prior to dilution and CD data collection. (C) The CD difference spectrum between the data in panel B is characteristic of the β-sheet, indicating an irreversible partial unfolding of the β-sheet structure in apoB.

double arrow) suggests a reduction in the solvent-exposed apolar surface, which may result from lipid coalescence and/or aggregation, rather than protein unfolding [the latter is characterized by $\Delta C_p > 0$ (*35*)]. Heating to 106 °C (completion of the second peak) eliminates this peak from the next scan (curve 4), indicating irreversibility of this transition, and also leads to a shift and broadening of the CE/TG peak (curves 4 and II). Thus, the altered packing of CE/TG is a result of the second high-temperature DSC transition.

To assess the effects of heating on the particle morphology, LDL samples of 3.3−3.7 mg/mL protein concentration were heated at 80−90 K/h from 20 to 75−115 °C, cooled and diluted 1:10, and visualized by EM at 22 °C (Figure 2). LDL heated to 75 °C (the onset of the first high-temperature DSC transition) appear as round particles, with diameters of 21−27 nm and an average $\langle d \rangle = 24.5$ nm, identical to those of intact LDL (Figure 2A). Heating to 85 °C (conclusion of the first DSC transition) converts a fraction of LDL into small LDL-like particles, large heterogeneous particles that are apparent products of LDL fusion, and their aggregates (Figure 2B). Also, short thin strands extending from the particles are observed, suggesting partial apoB dissociation. This trend continues upon heating to 100 °C (onset of the second high-temperature DSC peak), resulting in the predominance of the small LDL-like particles ($\langle d \rangle = 21.4$ nm), their aggregates, and large lipid droplets ($d = 30-100$ nm), along with thin strands with size and morphology that closely resemble delipidated apoB (*36*) (Figure 2C). This suggests that apoB dissociation is paralleled by LDL fusion into lipid droplets; similarly, LDL fusion may result from proteolytic degradation of apoB accompanied by dissociation of protein fragments (*37*, *38*). Heating to 115 °C (beyond the completion of the second DSC peak) leads to nearly complete conversion of the LDL-like particles into large aggregated lipid droplets (Figure 2D) that have size and morphology similar to the extracellular lipid deposits in atherosclerotic plaques (ref *39* and references cited therein). Taken together, our EM and DSC data suggest that the calorimetric transition at 82 °C leads to partial dissociation of apoB and to LDL rearrangement into smaller and larger particles (Figure 2B), while heating to higher temperatures leads to more extensive protein dissociation and fusion of the protein-depleted LDL into large aggregated droplets (Figure 2C,D).

To test whether the heat-induced LDL transitions involve apoB unfolding, far-UV CD spectra and the melting curves at 220 nm were recorded from LDL solutions of 40 μg/mL protein concentrations upon heating and cooling from 20 to 98 °C (Figure 3). The melting data show a gradual reduction in CD intensity, from $[\Theta_{220}(25\ °C)] = -24 \times 10^3$ deg·cm^2·dmol^{-1} to $[\Theta_{220}(98\ °C)] = -16 \times 10^3$ deg·cm^2·dmol^{-1} (Figure 3A), indicating a largely folded protein conformation at 98 °C (for heat-unfolded proteins, $[\Theta_{220}]$ may not exceed -5×10^3 deg·cm^2·dmol^{-1}). These CD changes are independent of the heating rate, as indicated by superimposition of the heating curves recorded at 11 and 80 K/h (Figure 3A), and are largely reversed upon cooling, as indicated by the agreement between the heating and cooling curves in Figure 3A and between the far-UV CD spectra of LDL recorded at 25 °C before and after heating to 99 °C (not shown). Such incomplete, noncooperative, largely reversible CD changes have also been observed in HDL (*29*) and are characteristic of the heat-induced structural relaxation rather than global protein unfolding.

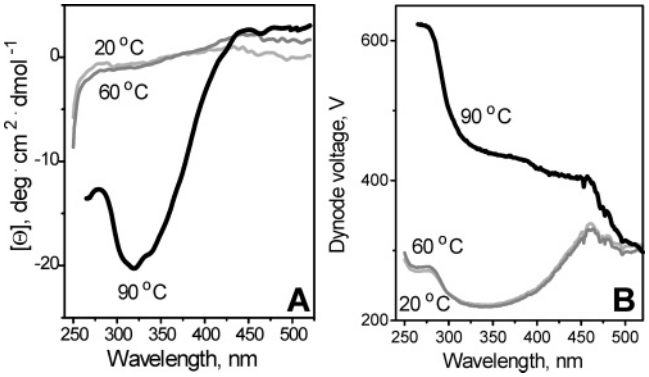

FIGURE 4: Heat effects on LDL near-UV/visible CD spectra (A) and turbidity monitored by dynode voltage in CD experiments (B). An LDL sample (3.7 mg/mL protein concentration) was equilibrated for 10 min at 20, 60, and 90 °C prior to CD data collection. Dynode voltage peaks near 280 and 460 nm correspond to absorption bands of protein and carotenoids (*40*), respectively; at 90 °C, the increase in the dynode voltage at all wavelengths reflects increase in the particle size.

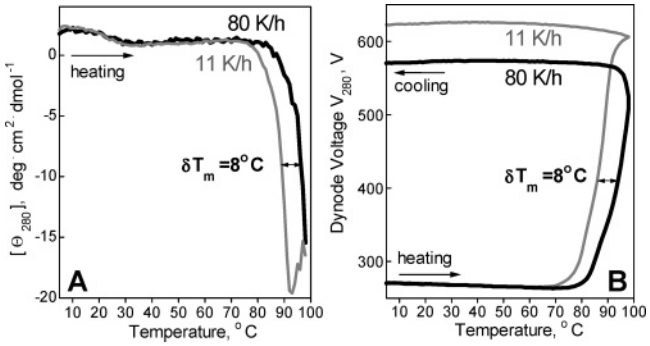

FIGURE 5: Scan rate effects on the near-UV CD and turbidity melting curves. The CD (A) and dynode voltage (turbidity) data (B) were recorded at 280 nm from LDL solutions (3.3 mg/mL protein concentration) during heating and cooling at 80 K/h (black line) and 11 K/h (gray line). Double arrows indicate shifts in the heating curves that result from the difference in the scan rate.

To test whether apoB unfolding occurs at higher temperatures and/or higher LDL concentrations, LDL samples of 3.3−3.7 mg/mL protein concentration were heated to 115 °C at 90 K/h in DSC experiments, cooled and diluted to 20−40 μg/mL protein concentration, and used to record far-UV CD and Trp emission spectra at 25 °C. The CD peaks at 193, 208, and 220 nm indicate ordered secondary structure comprised of α-helices and β-sheets (Figure 3B, gray line). Comparison with the far-UV CD of intact LDL (black line) shows spectral changes such as reduced CD intensity at 193 nm that cannot result from the heat-induced loss of LDL lipids [which may increase rather than reduce the CD signal at 193 nm (*40*)]; thus, these CD changes must reflect secondary structural changes in apoB. The difference spectrum between the CD of intact and heated LDL shows a positive band at 198 nm and a negative band at 218−221 nm characteristic of the β-sheet; consequently, heating to 115 °C leads to an irreversible loss of the β-sheet structure (Figure 3B). The Trp fluorescence spectrum of this sample recorded at 25 °C shows an irreversible red shift in the emission maximum from 340 to 346 nm (data not shown), indicating increased solvent exposure of Trp but not complete apoB unfolding (in unfolded proteins, exposed Trp shows maximal emission at 360 nm). No peak shift is observed upon LDL heating to 99 °C; consequently, Trp exposure in apoB is invariant up to 99 °C but increases at higher temperatures (115 °C). Taken together, our spectroscopic data show that LDL heating to 115 °C involves irreversible partial unfolding of β-sheets in apoB.

Near-UV/visible CD spectra of LDL were recorded upon heating from 10 to 90 °C. The spectra are nearly invariant at 20−70 °C, except for small changes near 30 °C reflecting CE/TG transition (*40*, *41*). However, heating to 90 °C induces a large negative CD peak at 320 nm (Figure 4A, black line) that must reflect altered packing of cholesterol, cholesterol esters, and/or carotenoids, which are the only LDL moieties that can exhibit induced CD near 320 nm (*42*−*44*). This heat-induced spectral change is not reversed upon cooling and is accompanied by a large irreversible increase in turbidity (Figure 4B, black line) that was monitored by dynode voltage in CD experiments (*31*). This increase is observed at any wavelength, from visible to far-UV, and becomes larger at shorter wavelengths, which is characteristic of light scattering. Also, LDL samples become visibly turbid after heating to 90 °C. Therefore, the heat-induced increase in turbidity reflects an increase in the particle size.

To correlate the heat-induced structural changes in LDL detected by different techniques, CD and turbidity melting curves, $\Theta_{280}(T)$ and $V_{280}(T)$, were recorded simultaneously at 280 nm under conditions (3.3 mg/mL LDL protein concentration, 80 K/h heating rate) similar to those used in DSC and EM experiments (Figures 1 and 2). Heating above 85 °C (beyond completion of the first DSC transition) leads to a large increase in the negative CD signal and in turbidity (black lines in Figure 5), indicating concomitant changes in the lipid packing and formation of larger particles and/or their aggregates. This spectroscopic transition apparently reflects conversion of intact LDL into heterogeneous LDL-like particles, large lipid droplets, and their aggregates observed by EM at these temperatures and LDL concentrations (Figure 2B,C).

To test whether this morphological transition is kinetically controlled, melting curves, $\Theta_{280}(T)$ and $V_{280}(T)$, of identical LDL samples were recorded at different scan rates. Slowing the heating from 80 to 10 K/h leads to a shift by about −8 °C in both CD and turbidity melting curves (gray and black lines in Figure 5). Such scan rate dependence indicates a slow kinetically controlled transition with high activation energy, $E_a \cong 60 \pm 20$ kcal/mol, that was estimated from the slope of the plot $\ln(\upsilon/T_m^2)$ versus $1/T$ (where υ is the scan rate and T is temperature in Kelvin) by using a kinetic approach of Sanchez-Ruiz (*31*, *45*).

Size comparison of intact LDL ($\langle d \rangle = 24.5$ nm) with large lipid droplets ($d = 30-100$ nm) in Figure 2A,D suggests that one such droplet is formed by coalescence of 5−200 LDL. To test the concentration dependence of this high-order reaction, we recorded CD and turbidity melting curves, $\Theta_{280}(T)$ and $V_{280}(T)$, from LDL samples of 1.5−4.0 mg/mL protein concentrations at a scan rate of 80 K/h. The $V_{280}(T)$ data show that increasing LDL concentration leads to large low-temperature shifts in the morphological transition (Figure 6) that are paralleled by similar shifts in $\Theta_{270}(T)$ data (not shown). Thus, at 1.5−2 mg/mL protein concentration, the transition is incomplete at 99 °C and the turbidity continues to increase even upon cooling from 99 °C (lines 1 and 2 in Figure 6), which is typical of slow kinetically controlled

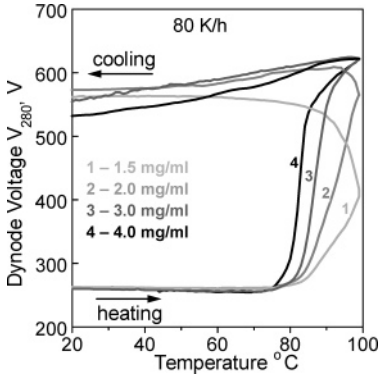

FIGURE 6: Effects of LDL concentration on the turbidity melting curves. The dynode voltage data were recorded in CD experiments at 280 nm upon heating LDL solutions of 1.5, 2.0, 3.0, and 4.0 mg/mL protein concentrations (curves 1−4) at 80 K/h.

reactions. In contrast, at 3−4 mg/mL protein concentrations, sigmoidal melting curves are observed (lines 3 and 4 in Figure 6), indicating that the transition is complete below 99 °C. Such concentration dependence confirms the high order of the heat-induced LDL fusion into aggregated lipid droplets.

To test whether the heat-induced structural changes in LDL involve oxidation and proteolysis (which is a marker of LDL oxidation), we used SDS and agarose gel electrophoresis and TLC to compare intact LDL with LDL heated to 115 °C. Intact and heated samples had identical TLC profiles that showed no additional lyso-PC or diene formation upon heating, indicating the absence of significant lipid oxidation. SDS gels of these samples were also identical, with a single band corresponding to full-size apo-B, indicating the absence of proteolysis. Agarose gel showed slightly increased electrophoretic mobility of the heated sample (ratio factor 0.14 compared to 0.1 for intact LDL), which may result from the conformational changes in apoB (Figure 3) and/or from mild oxidation. Also, UV absorption at 234 nm and ^{31}P NMR spectra remained invariant upon heating of intact LDL to the pretransitional temperature of 77 °C, indicating the absence of phospholipid oxidation (these spectra could not be reliably measured from thermally disrupted LDL because of increased turbidity). Consequently, oxidation may not be a driving force for the heat-induced morphological transitions in LDL.

DISCUSSION

Our results show for the first time that the thermal disruption of LDL is a complex high-order kinetically controlled transition that involves protein dissociation and changes in lipoprotein morphology but does not involve global protein unfolding. Earlier studies have attributed the first high-temperature DSC peak near 82 °C to irreversible apoB unfolding and LDL disruption (*17*−*25*). However, the CD and fluorescence data of this study clearly show that apoB does not unfold upon heating to 85 °C (Figure 3A). Furthermore, our EM data reveal changes in the particle size upon such heating that may result from the partial dissociation of apoB (Figure 2B). Similarly, thermal disruption of HDL does not involve global unfolding of apoA-1 that is prevented by the lipidated state of the dissociated protein (*29*). Thus, apoB unfolding in the high-temperature LDL transition is probably prevented by the lipidated protein state.

We also report an additional irreversible calorimetric LDL transition at higher temperatures. A similar double-peaked endotherm was observed in plasma HDL, with the second peak attributed to apoA-2 dissociation followed by particle rupture and coalescence of apolar lipids into droplets (*27*−*29*). The second high-temperature LDL transition may have a similar origin, since it is associated with (i) a shift and broadening of the CE/TG peak in the consecutive DSC scans (Figure 1, curves II and 4), indicating altered apolar lipid packing, (ii) a negative heat capacity increment, $\Delta C_p < 0$ (Figure 1, curves I and 3), suggesting lipid coalescence, (iii) conversion of most LDL into large lipid droplets and extensive dissociation of apoB detected by EM (Figure 2D), and (iv) partial β-sheet unfolding detected by CD (Figure 3B,C) and partial Trp exposure detected by fluorescence. In addition, this LDL transition is sensitive to LDL concentration (Figure 6) and to the thermal history of the sample (Figure 1, lines I and 3), indicating a high-order reaction with complex kinetics. In summary, the second high-temperature DSC transition in LDL apparently involves extensive dissociation of apoB and partial unfolding of its β-sheet structure, which leads to particle rupture and lipid coalescence into large droplets and their aggregates.

Fusion of the protein-depleted LDL into large aggregated lipid droplets above 80 °C (Figure 2C,D) causes a sharp increase in induced negative CD and in turbidity (Figures 4 and 5). Such morphological changes must involve transient disruption of the protein and/or lipid interactions, leading to high activation energy (enthalpy) of about 60 kcal/mol that is suggested by the scan rate effects on the CD and turbidity melting curves (Figure 5). Thus, similar to HDL, structural integrity of LDL is maintained by kinetic barriers. Similar energy barriers may separate discrete LDL subclasses in plasma and thereby modulate LDL metabolism. Kinetic barriers account for the structural stabilization and functional optimization of a variety of macromolecular systems (*30*, *46*−*48*) and confer resistance to destabilizing effects of irreversible protein alterations, such as oxidation and proteolysis (*48*). Our results suggest that the apoB-containing lipoproteins such as LDL may represent another class of macromolecular complexes whose structural integrity and resistance to the destabilizing effects of oxidation and proteolysis are kinetically controlled.

Large effects of LDL concentration on the CD and turbidity melting curves (Figure 6) suggest that the heat-induced LDL fusion is a high-order reaction. This is consistent with the particle size comparison (Figure 2A,D) suggesting that lipid droplet formation involves fusion of 5−200 LDL. Since the size and appearance of the aggregated lipid droplets in Figure 2D are remarkably similar to those of the extracellular lipid deposits in atherosclerotic arteries (ref *39* and references cited therein), the observed concentration dependence of the LDL-to-droplet conversion implies that a high-concentration setting, such as the arterial matrix, promotes fusion of modified LDL into lipid droplets.

A surprising observation is formation of small LDL-like particles upon LDL heating above 82 °C (Figure 2B,C); the properties of these particles and their possible relevance to small dense LDL will be explored. The heat-induced LDL size reduction by about 3 nm reported here resembles a similar 3 nm reduction due to phospholipid dissociation that occurs in the presence of free apoA-1 and fatty acids and is

proposed to contribute to LDL heterogeneity (*49*). Small dense LDL can also be generated from the medium-size LDL via the action of hepatic lipase or phospholipase A2 (*8*−*10*). The heat-induced formation of small LDL-like particles may mimic aspects of these metabolic reactions.

In summary, the heat-induced LDL size reduction and lipid droplet formation reported here may resemble aspects of metabolic LDL transformations in normal and in atherosclerotic states. In particular, heat-induced LDL fusion into lipid droplets reported here is a slow irreversible kinetically controlled reaction with high activation energy that arises from transient disruption of protein and lipid interactions. Similar kinetic factors may confer structural integrity to LDL in vivo and slow spontaneous morphological transitions such as fusion.

ACKNOWLEDGMENT

We thank Michael Gigliotti and Cheryl England for lipoprotein isolation, Chenghua Shao for help with the particle size analysis, and John Vural for help with NMR. We are indebted to Drs. Haya Herscovitz, Donald M. Small, and David Atkinson for expert advice.

REFERENCES

1. Atkinson, D., Deckelbaum, R. J., Small, D. M., and Shipley, G. G. (1977) Structure of human plasma low-density lipoproteins: molecular organization of the central core, *Proc. Natl. Acad. Sci. U.S.A. 74*, 1042−1046.
2. Hevonoja, T., Pentikainen, M. O., Hyvonen, M. T., Kovanen, P. T., and Ala-Korpela, M. (2000) Structure of low-density lipoprotein (LDL) particles: basis for understanding molecular changes in modified LDL, *Biochim. Biophys. Acta 1488*, 189−210.
3. Segrest, J. P., Jones, M. K., De Loof, H., and Dashti, N. (2001) Structure of apolipoprotein B-100 in low-density lipoproteins, *J. Lipid Res. 42*, 1346−1367.
4. Havel, R. J., and Kane, J. P. (2001) Structure and metabolism of plasma lipoproteins, in *The Metabolism & Molecular Bases of Inherited Disease*, 8th ed., Vol. II, McGraw-Hill, New York.
5. Kane, J. P., and Havel, R. J. (2001) Disorders of the biogenesis and secretion of lipoproteins containing the B apolipoproteins, in *The Metabolism & Molecular Bases of Inherited Disease*, 8th ed., Vol. II, McGraw-Hill, New York.
6. Goldstein, J. L., Hobbs, H. H., and Brown, M. S. (2001) Familial hypercholesterolemia, in *The Metabolism & Molecular Bases of Inherited Disease*, 8th ed., Vol. II, McGraw-Hill, New York.
7. Lusis, A. J. (2000) Atherosclerosis. *Nature 407*, 233−241.
8. Packard, C., Caslake, M., and Shepherd, J. (2000) The role of small, dense low-density lipoprotein (LDL): a new look, *Int. J. Cardiol. 74*, S17−S22.
9. Hurt-Camejo, E., Camejo, G., and Sartipy, P. (2000) Phospholipase A2 and small, dense low-density lipoprotein, *Curr. Opin. Lipidol. 11*, 465−471.
10. Hakala, J. K., Oorni, K., Pentikainen, M. O., Hurt-Camejo, E., and Kovanen, P. T. (2001) Lipolysis of LDL by human secretory phospholipase A2 induces particle fusion and enhances the retention of LDL to human aortic proteoglycans, *Arterioscler. Thromb. Vasc. Biol. 21*, 1053−1058; Guyton, J. R. (2001) *Arterioscler. Thromb. Vasc. Biol. 21*, 884−886 (comment).
11. Campos, H., Blijlevens, E., McNamara, J. R., Ordovas, J. M., Posner, B. M., Wilson, P. W., Castelli, W. P., and Schaefer, E. J. (1992) LDL particle size distribution. Results from the Framingham Offspring Study, *Arterioscler. Thromb. 12*, 1410−1419.
12. Berneis, K. K., and Krauss, R. M. (2002) Metabolic origins and clinical significance of LDL heterogeneity, *J. Lipid Res. 43*, 1363−1379.
13. McNamara, J. R., Small, D. M., Li, Z., and Schaefer, E. J. (1996) Differences in LDL subspecies involve alterations in lipid composition and conformational changes in apolipoprotein B, *J. Lipid Res. 37*, 1924−1935.
14. Williams, K. J., and Tabas, I. (1998) The response-to-retention hypothesis of atherogenesis reinforced, *Curr. Opin. Lipidol. 9*, 471−474.
15. Kruth, H. S. (1997) The fate of lipoprotein cholesterol entering the arterial wall, *Curr. Opin. Lipidol. 8*, 246−252.
16. Oorni, K., Pentikainen, M. O., Ala-Korpela, M., and Kovanen, P. T. (2000) Aggregation, fusion, and vesicle formation of modified low-density lipoprotein particles: molecular mechanisms and effects on matrix interactions, *J. Lipid Res. 41*, 1703−1714.
17. Deckelbaum, R. J., Shipley, G. G., Small, D. M., Lees, R. S., and George, P. K. (1975) Thermal transitions in human plasma low-density lipoproteins, *Science 190*, 392−394.
18. Deckelbaum, R. J., Shipley, G. G., and Small, D. M. (1977) Structure and interactions of lipids in human plasma low-density lipoproteins, *J. Biol. Chem. 252*, 744−754.
19. Ginsburg, G. S., Walsh, M. T., Small, D. M., and Atkinson, D. (1984) Reassembled plasma low-density lipoproteins. Phospholipid-cholesterol ester−apoprotein B complexes, *J. Biol. Chem. 259*, 6667−6673.
20. Walsh, M. T., and Atkinson, D. (1986) Physical properties of apoprotein B in mixed micelles with sodium deoxycholate and in a vesicle with dimyristoyl phosphatidylcholine, *J. Lipid Res. 27*, 316−325.
21. Walsh, M. T., and Atkinson, D. (1990) Calorimetric and spectroscopic investigation of the unfolding of human apolipoprotein B, *J. Lipid Res. 31*, 1051−1062.
22. Banuelos, S., Arrondo, J. L., Goni, F. M., and Pifat, G. (1995) Surface-core relationships in human low-density lipoprotein as studied by infrared spectroscopy, *J. Biol. Chem. 270*, 9192−9196.
23. Prassl, R., Schuster, B., Laggner, P., Flamant, C., Nigon, F., and Chapman, M. J. (1998) Thermal stability of apolipoprotein B100 in low-density lipoprotein is disrupted at early stages of oxidation while neutral lipid core organization is conserved, *Biochemistry 37*, 938−944.
24. Abuja, P. M., Lohner, K., and Prassl, R. (1999) Modification of the lipid−protein interaction in human low-density lipoprotein destabilizes ApoB-100 and decreases oxidizability, *Biochemistry 38*, 3401−3408.
25. Hammel, M., Laggner, P., and Prassl, R. (2003) Structural characterisation of nucleoside loaded low-density lipoprotein as a main criterion for the applicability as drug delivery system, *Chem. Phys. Lipids 123*, 193−207.
26. Chen, G. C., Chapman, M. J., and Kane, J. P. (1983) Secondary structure and thermal behavior of trypsin-treated low-density lipoproteins from human serum, studied by circular dichroism, *Biochim. Biophys. Acta 754*, 51−56.
27. Tall, A. R., Deckelbaum, R. J., Small, D. M., and Shipley, G. G. (1977) Thermal behavior of human plasma high-density lipoprotein, *Biochim. Biophys. Acta 487*, 145−153.
28. Tall, A. R., Puppione, D. L., Kunitake, S. T., Atkinson, D., Small, D. M., and Waugh, D. (1981) Organization of the core lipids of high-density lipoproteins in the lactating bovine, *J. Biol. Chem. 256*, 170−174.
29. Jayaraman, S., Gantz, D. L., and Gursky, O. (2004) Poly(ethylene glycol) induces fusion and destabilization of human plasma high-density lipoproteins, *Biochemistry 43*, 5520−5531.
30. Mehta, R., Gantz, D. L., and Gursky, O. (2003) Human plasma high-density lipoproteins are stabilized by kinetic factors, *J. Mol. Biol. 328*, 183−192.
31. Gursky, O., Ranjana, and Gantz, D. L. (2002) Complex of human apolipoprotein C-1 with phospholipid: thermodynamic or kinetic stability?, *Biochemistry 41*, 7373−7384.
32. Schumaker, V. N., and Puppione, D. L. (1986) Sequential flotation ultracentrifugation, *Methods Enzymol. 128*, 155−170.
33. Napoli, C., Postiglione, A., Triggiani, M., Corso, G., Palumbo, G., Carbone, V., Ruocco, A., Ambrosio, G., Montefusco, S., Malorni, A., Condorelli, M., and Chiariello, M. (1995) Oxidative structural modifications of low-density lipoprotein in homozygous familial hypercholesterolemia, *Atherosclerosis 118*, 259−273.
34. Karakatsani, A. I., Liapikos, T. A., Troganis, A. N., and Tsoukatos, D. C. (1998) Involvement of phospholipids in apolipoprotein B modification during low-density lipoprotein oxidation, *Lipids 33*, 1159−1162.
35. Privalov, P. L., and Makhatadze, G. I. (1992) Contribution of hydration and non-covalent interactions to the heat capacity effect on protein unfolding, *J. Mol. Biol. 224*, 715−723.
36. Gantz, D. L., Walsh, M. T., and Small, D. M. (2000) Morphology of sodium deoxycholate-solubilized apolipoprotein B-100 using

negative stain and vitreous ice electron microscopy, *J. Lipid Res. 41*, 1464−1472.
37. Piha, M., Lindstedt, L., and Kovanen, P. T. (1995) Fusion of proteolyzed low-density lipoprotein in the fluid phase: a novel mechanism generating atherogenic lipoprotein particles, *Biochemistry 34*, 10120−10129.
38. Pentikainen, M. O., Hyvonen, M. T., Oorni, K., Hevonoja, T., Korhonen, A., Lehtonen-Smeds, E. M., Ala-Korpela, M., and Kovanen, P. T. (2001) Altered phospholipid-apoB-100 interactions and generation of extra membrane material in proteolysis-induced fusion of LDL particles, *J. Lipid Res. 42*, 916−922.
39. Guyton, J. R., Klemp, K. F., and Mims, M. P. (1991) Altered ultrastructural morphology of self-aggregated low-density lipoproteins: coalescence of lipid domains forming droplets and vesicles, *J. Lipid Res. 32*, 953−962.
40. Chen, G. C., Krieger, M., Kane, J. P., Wu, C. S., Brown, M. S., and Goldstein, J. L. (1980) Beta-carotene as a probe of lipid domains of reconstituted human plasma low-density lipoprotein: induced circular dichroism, *Biochemistry 19*, 3330−3335.
41. Coronado-Gray, A., and van Antwerpen, R. (2003) The physical state of the LDL core influences the conformation of apolipoprotein B-100 on the lipoprotein surface, *FEBS Lett. 533*, 21−24.
42. Chen, G. C., and Kane, J. P. (1974) Contribution of carotenoids to the optical activity of human serum low-density lipoprotein, *Biochemistry 13*, 4706−4712.
43. Sklar, L. A., Craig, I. F., and Pownall, H. J. (1981) Induced circular dichroism of incorporated fluorescent cholesteryl esters and polar lipids as a probe of human serum low-density lipoprotein structure and melting, *J. Biol. Chem. 256*, 4286−4292.
44. Yeagle, P. L., Bensen, J., Greco, M., and Arena, C. (1982) Cholesterol behavior in human serum lipoproteins, *Biochemistry 21*, 1249−1254.
45. Sanchez-Ruiz, J. M. (1992) Theoretical analysis of Lumry-Eyring model in differential scanning calorimetry, *Biophys. J. 61*, 921−935.
46. Baker, D. (1998) Metastable states and folding free energy barriers, *Nat. Struct. Biol. 5*, 1021−1024.
47. Jaswal, S. S., Sohl, J. L., Davis, J. H., and Agard, D. A. (2002) Energetic landscape of alpha-lytic protease optimizes longevity through kinetic stability, *Nature 415*, 343−346.
48. Plaza del Pino, I. M., Ibarra-Molero, B., and Sanchez-Ruiz, J. M. (2000) Lower kinetic limit to protein thermal stability: a proposal regarding protein stability in vivo and its relation with misfolding diseases, *Proteins 40*, 58−70.
49. Musliner, T. A., Long, M. D., Forte, T. M., and Krauss, R. M. (1991) Size transformations of intermediate and low-density lipoproteins induced by unesterified fatty acids, *J. Lipid Res. 32*, 903−915.

BI047493V